Overcoming gefitinib resistance and metastasis in adenocarcinoma through synergistic PI3K–AKT–ERK blockade: Integrated rational co-delivery nanoplatform and multimodel validation

Jialong Deng[1,2#], Bin Xu[3#], Huili Wang[4#], Weihuan Lin[5], Hengliang Hou[2,3], Shengbo Liu[1,2], Yucheng Huang[2,3], Zenan Lin[2], Qiaxuan Li[2], Hongrui Qiu[2,4], Chaodong Wu[6], Yubo Zhou[7], Fanjun Zeng[5*], Lintong Yao[2*], and Haiyu Zhou[2*]

ABSTRACT

Hyperactivation of the phosphatidylinositol 3-kinase (PI3K)–protein kinase B (AKT) pathway, a key downstream effector of the epidermal growth factor receptor (EGFR), drives resistance to EGFR tyrosine kinase inhibitors (TKIs) in lung adenocarcinoma by promoting cell proliferation and metastasis, often compounded by compensatory pathway activation. Integrated analysis of Gene Expression Omnibus datasets confirmed PI3K/AKT hyperactivation in resistant tumors. Drug synergy analysis revealed a potent interaction between gefitinib and crizotinib (Crz). Mechanistic studies using phospho-proteomics showed that Crz co-treatment synergistically suppresses both PI3K/AKT and compensatory extracellular signal-regulated protein kinases activation, significantly inhibiting the proliferation and invasion of PC-9 gefitinib-resistant cells. *In vivo* validation using xenografts and zebrafish metastasis models demonstrated that this combination strategy overcomes drug resistance and inhibits metastasis. To optimize pharmacokinetic coordination and efficacy, dual drug-loaded poly (ethylene glycol)–poly (hexyl ethylene phosphate) nanoparticles with high loading capacity were engineered. In this multiscale study, we established rationally designed nanocarriers for a dual-pathway blockade as a transformative strategy against TKI resistance, providing a clinically translatable platform for overcoming metastatic progression.

Keywords:
Lung adenocarcinoma; Gefitinib resistance; Crizotinib; Phosphatidylinositol 3-kinase–protein kinase B signaling; Nanoparticles

*Authors contributed equally.

***Corresponding authors:**
Fanjun Zeng,
zengfanjun@gdph.org.cn;
Lintong Yao,
ltyao2023@i.smu.edu.cn;
Haiyu Zhou,
zhouhaiyu@gdph.org.cn

How to cite this article:
Deng J, Xu B, Wang H, *et al.* Overcoming gefitinib resistance and metastasis in adenocarcinoma through synergistic PI3K–AKT–ERK blockade: Integrated rational co-delivery nanoplatform and multimodel validation. *Biomater Transl.* 2026.

doi: 10.12336/bmt.25.00173

1. Introduction

Lung cancer, a highly malignant tumor with a poor prognosis, has the highest incidence and mortality among all cancers.[1] Approximately 85% of these cases are non-small cell lung cancers (NSCLCs).[2] Despite advancements in treatment strategies, achieving long-lasting therapeutic effects remains challenging because of inherent tumor cell mutations or the development of resistance following drug treatment.[3] Drug resistance is a considerable factor in tumor progression and recurrence.[4] The epidermal growth factor receptor (EGFR), a tyrosine kinase receptor, is the most frequent driver of NSCLC. Tyrosine kinase inhibitors (TKIs) have demonstrated efficacy in treating EGFR-mutated advanced NSCLC, particularly in lung adenocarcinoma, a common subtype of NSCLC. Gefitinib (Gef), a first-generation EGFR-TKI, has shown promising therapeutic potential in patients with EGFR-mutated NSCLC, yet resistance to Gef therapy is an inevitable issue.[5] Consequently, exploring innovative treatment

strategies that build upon EGFR-TKI treatment to enhance the survival rates of patients with drug-resistant disease remains an urgent priority.

Combining multiple drugs, such as cyclosporin A,[6] chloroquine,[7] and rapamycin,[8] can potentially overcome Gef resistance through synergistic effects that target survival pathways in resistant tumor cells. However, the clinical efficacy of these combination therapies is often limited by poor tumor targeting and inadequate uptake of small-molecule drugs by tumor cells following intravenous administration.[9] Therefore, developing a clinically viable strategy to enhance treatment efficacy remains an urgent need. Currently, nanotechnology has been widely applied in tumor drug delivery and holds significant potential for addressing the limitations of small molecule drugs, including various "all-in-one" theranostic strategies.[10] Additionally, in our previous work, we have achieved efficient delivery of EGFR-TKIs using a polyphosphoester-based material.[11] These findings collectively lay a solid foundation for the present study, which aims to target key resistance-related signaling pathways in NSCLC.

The phosphatidylinositol 3-kinase (PI3K)–protein kinase B (AKT) pathway, a downstream effector of EGFR, plays a crucial role in regulating tumor cell proliferation, migration, and survival.[12-17] This pathway has been implicated in the development of Gef resistance[18-21] and brain metastasis of lung cancer.[22-24] Crizotinib (Crz), a clinically approved TKI, is often used to treat patients with locally advanced or metastatic NSCLC harboring echinoderm microtubule-associated protein-like 4-anaplastic lymphoma kinase fusion.[25] Crz has been shown to effectively inhibit AKT phosphorylation in ovarian cancer and rhabdomyosarcoma cells[26,27] and has been used in combination with Gef to treat patients with EGFR-TKI resistance associated with epithelial–mesenchymal transition (EMT) amplification.[28]

In this study, we hypothesized that the synergistic inhibition of the PI3K/AKT pathway, along with suppression of extracellular signal-regulated kinase (ERK) signaling, could be achieved by combining Gef and Crz to overcome Gef resistance and mitigate metastasis in lung adenocarcinoma. Our experiments using a zebrafish xenograft model demonstrated the potent efficacy of this dual-drug therapy in suppressing tumor growth and spread. To support our hypothesis and highlight the relationships between Gef and Crz, we designed a poly (ethylene glycol) (PEG)–poly (hexyl ethylene phosphate) (PHEP) polymer-based nanocarrier (PEG–PHEP@Gef/Crz) for co-delivery, with the aim of prolonging drug circulation and enhancing tumor targeting in EGFR-mediated Gef-resistant lung adenocarcinoma.

The PEG–PHEP@Gef/Crz nanocarrier ensures stable *in vivo* circulation owing to the PEG shell and accumulates in tumors owing to the enhanced permeability and retention effect following intravenous injection. This system promotes the uptake of Gef and Crz by tumor cells via endocytosis, leading to the release of the encapsulated drugs. By inhibiting AKT phosphorylation and inducing apoptosis, this delivery system not only hinders cancer cell survival but also reduces metastasis to critical organs such as the lungs and liver.

In summary, the present study provides valuable insights into novel approaches to combat drug resistance in lung adenocarcinoma by precisely targeting molecular pathways, thereby laying the foundation for more effective treatment strategies.

2. Materials and methods

2.1. Materials

Gefitinib was purchased from Selleck Co. Ltd., China. Crz was obtained from Thain Chemical Technology Co., Ltd., China. Antibodies against AKT/phosphorylated-AKT (#4691, #4060, Cell Signaling Technology Co. Ltd., USA), ERK/phosphorylated-ERK (#4695,#4370., Cell Signaling Technology Co. Ltd., USA), β-tubulin (#2146, Cell Signaling Technology Co. Ltd., USA), and β-actin (#4970, Cell Signaling Technology Co. Ltd., USA) were purchased from Cell Signaling Technology Co. Ltd., United States of America (USA). Cell Counting Kit-8 (CCK-8) was purchased from Biosharp Co., Ltd., China (#BS350). EdU Imaging Kit was obtained from APExBIO, USA (HF594). 1,1'-dioctadecyl-3,3,3',3'-tetramethylindocarbocyanine perchlorate (DiI) was purchased from Thermo Fisher Scientific Inc., USA. SC79 (AKT activator) was obtained from Beyotime Biotechnology Co., Ltd., China. Other chemicals and reagents were of analytical grade and used without modification.

2.2. Cell lines and animals

PC-9, Gef-resistant PC-9 (PC9GR), A549, and Gef-resistant A549 (A549GR) cells were obtained from the American Type Culture Collection, USA. Cells were cultured with complete Roswell Park Memorial Institute (RPMI) 1640 medium containing 10% fetal bovine serum (FBS), 1% (v/v) penicillin–streptomycin, and the remaining 89% RPMI 1640 medium. Cells were cultured in an incubator with 5% CO_2 at 37°C.

Zebrafish strains were obtained from the China Zebrafish Resource Center, Wuhan, China, and maintained in an aerated flow-through tank within a light–dark cycle of 14:10 h. Water parameters were maintained at pH 7.0 ± 0.5, conductivity of 500–600 μS/cm, and temperature of 28°C ± 1°C. A female and

[1]School of Medicine, South China University of Technology, Guangzhou, Guangdong, China; [2]Department of Thoracic Surgery, Guangdong Provincial People's Hospital (Guangdong Academy of Medical Sciences), Southern Medical University, Guangzhou, Guangdong, China; [3]School of Biomedical Sciences and Engineering, South China University of Technology, Guangzhou International Campus, Guangzhou, Guangdong, China; [4]Department of Thoracic Surgery, Guangdong Provincial People's Hospital (Guangdong Academy of Medical Sciences), Guangzhou University of Chinese Medicine, Guangzhou, Guangdong, China; [5]Department of General Practice, Guangdong Provincial Geriatrics Institute, Guangdong Provincial People's Hospital, Guangdong Academy of Medical Sciences, Southern Medical University, Guangzhou, Guangdong, China; [6]The First Clinical Medical School, Southern Medical University, Guangzhou, Guangdong, China; [7]School of Chinese Medicine, Faculty of Medicine, Macao University of Science and Technology, Macao, China

male zebrafish were placed in the breeding tanks after feeding and separated by a partition. The partition was removed after 10 h of darkness, and the breeding was induced in the morning by switching on the light. Approximately 2.5 h later, embryos were collected, rinsed with pure water, and placed into the embryo incubator for subsequent experiments. Female BALB/c nude mice (5 weeks old, 18–22 g, $n = 25$) were purchased from Hunan SJA Laboratory Animal Co., Ltd, China. All animals were cared for in accordance with the Guide for the Care and Use of Laboratory Animals. The procedures used in this study were approved by the Ethics Committee of Guangdong Provincial People's Hospital.

2.3. Bioinformatic analysis

We used GSE169513 (public RNA-sequencing datasets of PC9GR and PC-9 cells), GSE129221 (public RNA-sequencing datasets of PC9GR and PC-9 cells), and GSE83132 (public RNA-sequencing datasets of PC-9 brain metastasis cells and PC-9 cells), which were downloaded from the Gene Expression Omnibus. For data analysis, we used the Limma package to identify differentially expressed genes (DEGs) ($|\log_2$ fold change$| \geq 1$ and $p<0.05$), which were subsequently used for gene ontology (GO) analysis and Kyoto Encyclopedia of Genes and Genomes (KEGG) pathway enrichment analysis. All bioinformatic analyses were performed in R software (version 4.3.1, R Foundation for Statistical Computing, Austria).

2.4. Determination of drug resistance factor

To determine the drug resistance of PC9GR to Gef, PC-9 and PC9GR cells were resuspended in complete RPMI 1640 medium at 5×10^4 cells/mL, and 0.1 mL cell suspension was seeded into each well of 96-well plates and incubated overnight. Subsequently, the culture medium was replaced with an equal volume of fresh media containing different concentrations of Gef (10^{-6}–10^2 μM). After incubation for 24 h, the viability of PC-9 and PC9GR cells under different Gef concentrations was measured using the CCK-8 assay with a microplate reader (Thermo Fisher Scientific, USA).

2.5. Cell proliferation assay

PC-9 Gef-resistant cells were resuspended in complete RPMI 1640 medium at 5×10^4 cells/mL, and 0.1 mL of cell suspension was seeded into each well of 96-well plates. After 24 h, cells were incubated with fresh media containing 2 μM Gef, 2 μM Crz, and 2 μM Gef + 2 μM Crz. Cell viability after treatment for 0, 24, and 48 h was measured using the CCK-8 assay with a microplate reader (Thermo Fisher Scientific, USA). In addition, the EdU Imaging kit was used to assess cell antiproliferation, which was subsequently imaged using a fluorescence microscope (Zeiss, Germany).

2.6. Cell migration assay

The scratch wound-healing migration assay was used to evaluate the inhibition of cell migration with Gef + Crz. PC9GR cells were seeded into 6-well plates at 1.5×10^6 cells per well in 2 mL complete RPMI 1640 medium and incubated overnight. Subsequently, after the cells reached >90% confluency, phosphate-buffered saline (PBS) was used to wash the cell surface twice, and then three uniform lines were scratched with a 200-μL sterile micropipette tip. PBS was used to wash away detached cells, and complete RPMI 1640 medium with 1% FBS containing different drugs (0.5 μM Gef, 0.5 μM Crz, or 0.5 μM Gef + 0.5 μM Crz) was added. The cells were then incubated for 24 h. Finally, the scratched lines were imaged using an inverted microscope (DM IL, Leica, Germany).

2.7. Quantitative real-time polymerase chain reaction

PC-9 Gef-resistant cells were cultured overnight in 6-well plates. Following the addition of 0.5 μM Gef + 0.5 μM Crz, cells were further cultured for 48 h before collection. Total RNA was extracted from cells using TRIzol reagent (Life Technologies, Carlsbad, USA) following the manufacturer's protocol. Complementary DNA was synthesized using MMLV reverse transcriptase for quantitative real-time polymerase chain reaction (qPCR) (Promega, USA). qPCR was conducted on a LightCycler 96 system (Roche Diagnostics, USA) using SYBR Green Master Mix (Applied Biosystems, USA). Gene expression values were normalized to glyceraldehyde-3-phosphate dehydrogenase (*GAPDH*) as a housekeeping gene. The primer sequences are presented in Table S1.

2.8. Cell apoptosis assay

For the apoptosis assay, PC9GR cells were incubated with 2 μM Gef, 2 μM Crz, or 2 μM Gef + 2 μM Crz for 24 h. The cells were then collected and stained with Annexin V-FITC apoptosis detection kit C1062, Beyotime, Shanghai, China and analyzed by fluorescence-activated cell sorting (FACS; BD Biosciences, USA).

2.9. *In vitro* antitumor mechanism

Western blotting and acridine orange (AO) staining were employed to investigate the antitumor mechanism of the Gef + Crz combination. PC9GR cells were cultured in complete RPMI 1640 medium containing Gef + Crz (2 μM) for 24 h. Total protein was extracted from the collected cells, and protein concentration was quantified using the bicinchoninic acid assay. Equal amounts of protein were subjected to standard western blotting, followed by incubation with the primary antibodies against AKT, p-AKT, β-actin, ERK, p-ERK, and β-tubulin at 4°C under gentle agitation overnight. After three washes, the membranes were incubated with the corresponding secondary antibody at room temperature for 1 h. Immunoreactive bands on polyvinylidene fluoride membranes were visualized using chemiluminescence.

In addition, SC79 (10 μM), an AKT pathway activator, was used to reverse the apoptosis induced by Gef + Crz. Following 24 h of incubation, PC9GR cells were stained with AO in the dark for 15 min. After three washes with PBS containing 3% bovine serum albumin, cells were imaged using a fluorescence microscope (Zeiss, Germany).

2.10. Antitumor effects of Gef + Crz in zebrafish embryos

A zebrafish xenograft model was used to evaluate the *in vivo* antitumor effects of Gef + Crz. Approximately 200 DiI-stained

PC9GR cells were injected into the common cardinal vein of *Tg*(*fli*: eGFP) zebrafish embryos at 2 days post-fertilization (dpf). After 6 h, 1 nL of drug solution (0.5 μM Gef, 0.5 μM Crz, or 0.5 μM Gef + 0.5 μM Crz) was injected into the same site. Subsequently, embryos were incubated in a 34°C incubator, and the medium was replaced daily with fresh E3 medium (5 mM sodium chloride, 0.17 mM potassium chloride, 0.33 mM calcium chloride, and 0.33 mM magnesium sulfate); 0.2 mM N-phenylthiourea (Sigma-Aldrich, USA) was added from 1 dpf to inhibit pigmentation. Metastatic tumor cells in the embryo tails were imaged using fluorescence microscopy at 3 days post-injection, and distal metastatic lesions were further imaged at 4 days post-injection.

2.11. Nanoparticle synthesis and preparation

The amphiphilic block copolymer PEG–PHEP was synthesized according to a previously reported method[29] and used to co-load Gef and Crz into nanoparticles (PEG–PHEP@Gef/Crz). Specifically, Gef (0.5 mg), Crz (0.5 mg), and PEG–PHEP (10 mg) were dissolved in 0.6 mL of tetrahydrofuran. The solution was added dropwise to 3.6 mL of water and stirred at 600 rpm for 5 h. After stirring, tetrahydrofuran was completely removed using a rotary evaporator, and the resulting suspension was further stirred overnight at room temperature. Finally, the solution was centrifuged at 5,000 rpm for 5 min to remove unloaded free drug, and the collected supernatant was designated PEG–PHEP@Gef/Crz.

Nanoparticles loaded with a single drug, termed PEG–PHEP@Gef and PEG–PHEP@Crz, were prepared by modifying the formulation to 1 mg Gef + 10 mg PEG–PHEP or 1 mg Crz + 10 mg PEG–PHEP, respectively.

2.12. Nanoparticle characterization

After dilution with water, the hydrodynamic size of PEG–PHEP@Gef/Crz was measured using dynamic light scattering (Zetasizer Nano ZSE, Malvern Instruments, UK) at 25°C. Successful drug loading was confirmed by measuring the ultraviolet-visible spectra of PEG–PHEP@Gef/Crz using an ultraviolet spectrophotometer (UV-1280, Shimadzu, Japan). The stability of PEG–PHEP@Gef/Crz was assessed by monitoring changes in particle size at 0, 12, 24, 36, 48, and 60 h during incubation in 1×PBS, PBS containing 10% FBS, and complete RPMI 1640 medium. Encapsulation efficiency of PEG–PHEP@Gef/Crz was quantified using high-performance liquid chromatography.

2.13. Nanoparticle uptake

Coumarin 6 (C6; MedChemExpress, USA) was used as a fluorescent probe to label the nanoparticles and was encapsulated in their core. PC9GR cells were resuspended in complete RPMI 1640 medium at 5×10^4 cells/mL, and 2 mL of the cell suspension was seeded into each well of a 6-well plate. Following cell adhesion, the fluorescently labeled nanoparticles were incubated with PC9GR cells for 0.5, 1, 2, 3, and 4 h at 37°C under 5% CO_2. Cells in each treatment group were harvested, washed twice with PBS, and resuspended in 0.5 mL PBS. Intracellular fluorescence intensity was quantified by FACS analysis using an Accuri C6 flow cytometer (BD Biosciences, USA), and the intracellular localization of PEG–PHEP@Gef/Crz was visualized by confocal laser scanning microscopy (CLSM; Leica, Germany).

After 2 h of incubation with the fluorescently labeled nanoparticles, the culture medium was removed, and cells were gently washed three times with PBS and fixed with 4% paraformaldehyde for 10 min. Cells were subsequently washed three times with PBS and permeabilized with 0.3% Triton X-100 (Sigma-Aldrich, USA) in PBS for 15 min. Hoechst dye was used to stain cell nuclei for 5 min. Finally, PBS was used to remove residual surface-bound dye, and the cells were imaged using CLSM (ICS SP8, Leica, Germany).

2.14. Antitumor effects of PEG–PHEP@Gef/Crz in nude mice

PC-9 Gef-resistant xenograft tumor (~50 mm^3)-bearing BALB/c nude mice (n = 25) were randomly divided into five groups (n = 5 per group) and intravenously administered PBS, PEG–PHEP@Gef, PEG–PHEP@ Crz, Gef + Crz, or PEG–PHEP@Gef/Crz at a Gef dose of 2 mg/kg and Crz dose of 2 mg/kg every 3 days. Tumor length and width, as well as body weight, were measured every 3 days. After 15 days of treatment, the mice were humanely euthanized, and tumor tissues were excised and weighed. The tumors were then fixed, paraffin-embedded, and sectioned for histopathological evaluation. Hematoxylin and eosin (H&E) staining was performed to assess tissue morphology, and immunohistochemical analyses, including terminal deoxynucleotidyl transferase dUTP nick end labeling and Ki-67 staining, were conducted to evaluate apoptosis and cell proliferation, respectively.

2.15. Biosafety assessment

After treatment, the mice were humanely euthanized, and whole blood samples were collected. Following centrifugation at 14,000 rpm for 10 min, the serum was isolated for routine blood tests and biochemical analysis. Major organ tissues were harvested, paraffin-embedded, sectioned, and stained with H&E to evaluate treatment-related histopathological changes.

2.16. Transcriptomic mRNA sequencing analysis

Tumor tissues were collected from mice treated with PBS or PEG–PHEP@Gef/Crz for mRNA sequencing analysis. Raw sequencing data were processed through data cleaning, quality control, and normalization to fragments per kilobase of transcript per million mapped reads, resulting in the identification of 16,319 annotated mRNA transcripts. A total of 731 DEGs were identified using the limma package in R software, providing the basis for subsequent functional enrichment analyses using GO and KEGG pathways. Gene set enrichment analysis (GSEA) was performed using the annotated gene set "c2.cp.kegg_medicus.v2024.1.Hs.symbols.gmt" from the Molecular Signatures Database.

2.17. Statistical analysis

Statistical analyses were conducted using GraphPad Prism version 9.0 (USA). Data are presented as mean ± standard

deviation. Differences between two groups were evaluated using Student's *t*-test. A $p<0.05$ was considered statistically significant.

3. Results

3.1. PI3K/AKT signaling is hyperactivated in Gef-resistant lung adenocarcinoma cells

Previous studies have demonstrated that activation of alternative EGFR downstream pathways, such as signal transducers and activators of transcription 3[6,30] and PI3K/AKT,[21,22] is linked to resistance to EGFR-TKIs. Analysis of RNA-sequencing data from public datasets revealed 4,163 DEGs in PC9GR versus PC-9, with 2,614 upregulated and 1,549 downregulated genes in GSE169513 datasets (**Figure 1A**). Additionally, GSE129221 revealed 2,661 differential genes, of which 1,530 were upregulated, and 1,131 were downregulated (**Figure 1B**). The intersection of these datasets identified 537 common differential genes (**Figure 1C**). GO annotation functional analysis revealed that the DEGs were significantly associated with the regulation of key pathways, including the mitogen-activated protein kinase pathway, Wnt signaling, erythroblastic leukemia viral oncogene homolog signaling, and transforming growth factor-β signaling. These pathways are integral to the modulation of intracellular signaling cascades and are closely linked to cellular survival and proliferative processes (**Figure 1D**). KEGG pathway enrichment analysis indicated that the DEGs were predominantly engaged in the PI3K/AKT signaling pathway and focal adhesion, and were also implicated in resistance to EGFR-TKIs (**Figure 1E**).

These findings suggest that the PI3K/AKT signaling pathway plays a crucial role in mediating Gef resistance in lung

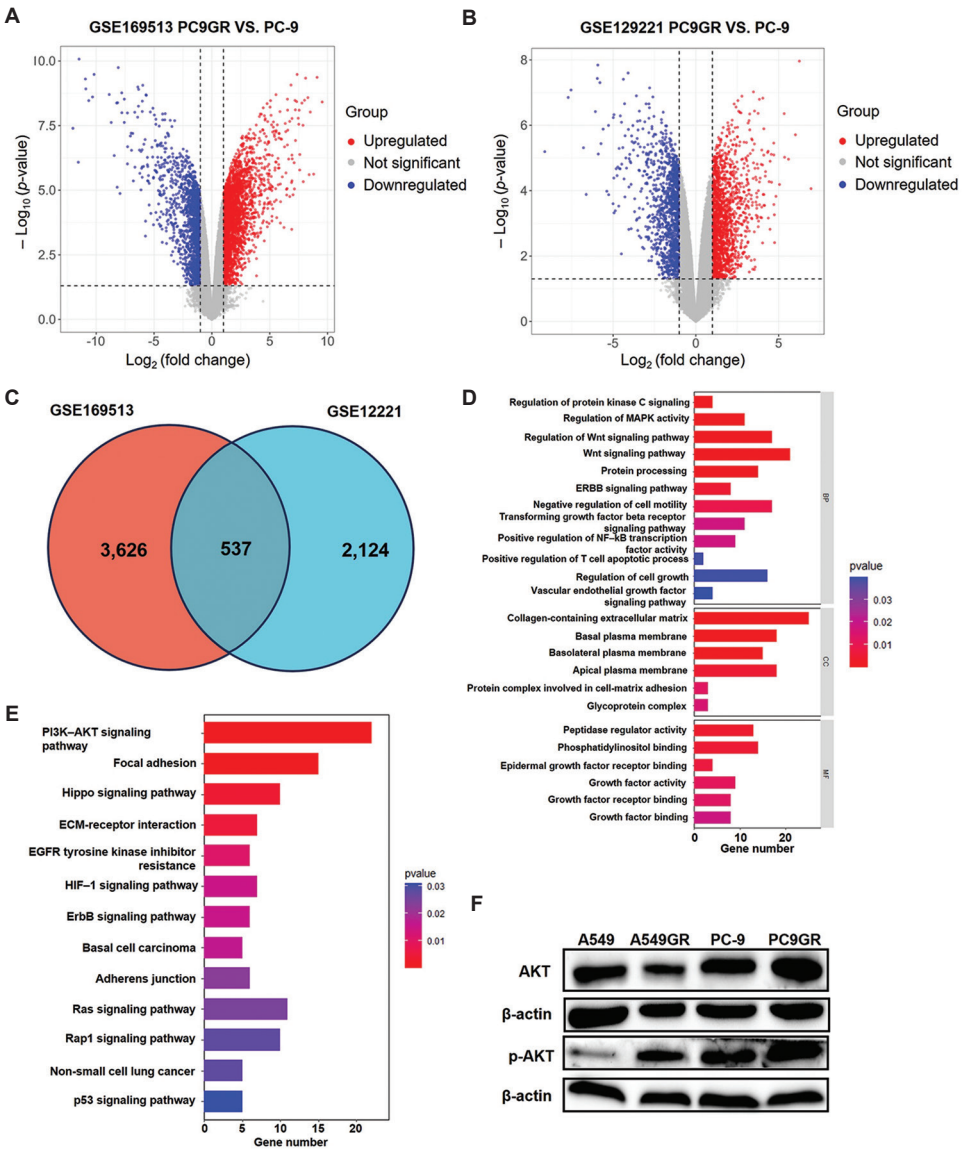

Figure 1. Analysis of gene expression analysis and signaling in PC9GR versus PC-9 cells. Volcano plots showing differential gene expression in the (A) GSE169513 and (B) GSE129221 datasets. (C) Venn diagram illustrating the overlap of differential expressed genes between the two datasets, revealing 537 shared genes. (D) Gene Oncology annotation and (E) Kyoto Encyclopedia of Genes and Genomes pathway enrichment analysis of the differentially expressed genes. (F) Immunoblot analysis of AKT and p-AKT levels in gefitinib-resistant and parental PC-9 cells. Abbreviations: AKT: Protein kinase B; p-AKT: Phosphorylated protein kinase B; PC9GR: Gefitinib-resistance PC-9 cell.

adenocarcinoma. Subsequent analysis of AKT signaling in Gef-resistant versus primary lung adenocarcinoma cell lines revealed markedly elevated p-AKT levels in the resistant cells, suggesting that PI3K/AKT signaling is hyperactivated in drug-resistant cell lines (**Figure 1F**). Collectively, these findings underscore the importance of targeting PI3K/AKT as a strategy for overcoming drug resistance.

3.2. Gef + Crz synergistically inhibits proliferation and migration of PC9GR cells

To determine the resistance coefficient of PC9GR cells, the cells were analyzed using a cytotoxicity assay. The results showed that the IC_{50} (half-maximal inhibitory concentration) of Gef for PC-9 and PC9GR cells was 0.078 μM and 5.9 μM, respectively, suggesting that the resistance coefficient of PC9GR was 75.6 (Figure S1).

To determine the optimal combination ratio of Gef and Crz, we performed a drug synergy coefficient analysis. The cytotoxic effects of different drug concentrations on PC9GR cells are shown in **Figure 2A**. Further evaluation yielded a zero interaction potency synergy score of 5.866 for the drug pair, indicating a robust synergistic interaction. The most pronounced synergistic cytotoxicity was achieved using an equal ratio of Gef to Crz (**Figure 2B**).

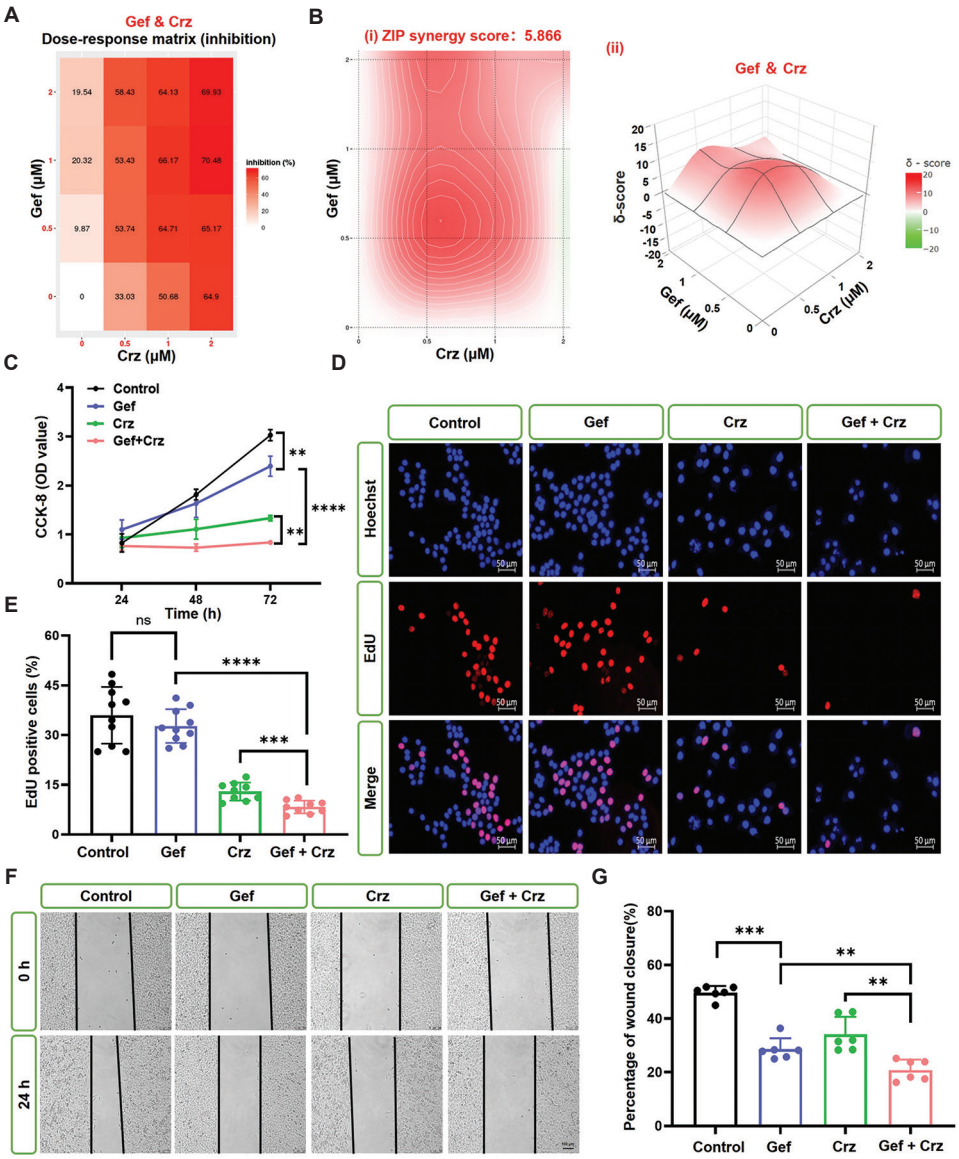

Figure 2. Gef combined with Crz synergistically inhibits the proliferation and migration of PC9GR cells. (A) Drug response matrix showing the inhibitory effect of Gef in combination with Crz on PC9GR cells; each value represents the percentage inhibition. (B) ZIP synergy scores analyzed in (i) two-dimensional and (ii) three-dimensional plots; regions with δ-scores > 10 indicate strong synergistic drug synergy. (C) CCK-8 assay measuring PC9GR cell proliferation under different treatments; OD values reflect viable cell numbers. (D) Representative EdU staining images (scale bar = 50 μm; magnification = 20×) and (E) corresponding quantification of DNA synthesis in PC9GR cells. (F) Scratch assay and (G) quantification of cell migration after treatment with different formulations. Data are presented as mean ± standard deviation. Statistical significance was assessed using an unpaired Student's *t*-test. ***p*<0.01, ****p*<0.001, and *****p*<0.0001 indicate statistical significance; "ns" indicates no significant difference.

Abbreviations: CCK-8: Cell counting kit 8; Crz: Crizotinib; Gef: Gefitinib; OD: Optical density; ZIP: Zero interaction potency.

Based on these findings, our subsequent combination therapy experiments used equal concentrations of Gef and Crz. Next, the cytotoxicity of different concentrations of Gef + Crz (0.25 to 8 μM) in PC9GR cells was assessed using the CCK-8 assay. The Gef + Crz group exhibited maximal antitumor activity, whereas Gef alone caused <50% cell death even at 8 μM, indicating that Gef and Crz exert a synergistic cytotoxic effect on PC9GR cells (Figure S2).

Considering that PI3K/AKT signaling is involved in the proliferation and migration of tumor cells,[14-16] we first assessed the effect of different drug combinations on PC9GR cell proliferation. The CCK-8 cytotoxicity results and EdU assay indicated that the combination therapy substantially inhibited PC9GR cell proliferation (**Figure 2C-E**). Furthermore, we evaluated the migration rate of PC9GR cells after treatment with the different formulations. Gef + Crz produced the lowest migration rate compared with Gef or Crz alone, confirming that Gef + Crz combination achieves a combined inhibitory effect (**Figure 2F** and **G**). Interestingly, Gef inhibited the migratory ability of PC9GR cells more effectively than Crz at 0.5 μM. Overall, combination therapy with Gef and Crz effectively inhibited the proliferation and migration of PC9GR cells.

To verify whether the synergistic blockade of the PI3K/AKT–ERK pathway inhibits tumor cell invasion through regulation of EMT, we assessed the expression of key EMT markers (e.g., E-cadherin, vimentin, Snail) via qPCR. As shown in Figure S3, compared with the control group, combined treatment with Gef and Crz did not induce significant changes in the expression of E-cadherin or Snail. Although a modest reduction in vimentin expression was observed, this isolated change was insufficient to indicate a systemic or functional EMT transition. Furthermore, N-cadherin expression remained below the detection limit.

Collectively, these findings suggest that the inhibitory effect of synergistic PI3K/AKT–ERK pathway blockade on tumor cell invasion and metastasis is primarily mediated through pathways distinct from classical EMT. The minor adjustment in vimentin expression may reflect a partial, non-dominant involvement in EMT-related processes, whereas other mechanisms—such as regulation of cell adhesion, extracellular matrix degradation, or alternative signaling cascades beyond the EMT axis—likely constitute the primary contributors to the observed anti-invasive effects.

3.3. Gef + Crz synergistically inhibits PI3K/AKT signaling and suppresses ERK signaling feedback activation to induce apoptosis in PC9GR cells

The PI3K/AKT signaling is indispensable for numerous cellular activities, including tumor cell survival and apoptosis.[13-15] In this study, we measured apoptosis in PC9GR cells treated with different formulations. The findings revealed that treatment with 2 μM Gef for 24 h did not significantly increase apoptosis compared with control, indicating that PC9GR cells were resistant to Gef.

Conversely, Gef + Crz treatment significantly induced apoptosis in PC9GR cells (**Figure 3A** and **B**). Notably, the cytotoxicity of Gef was lower than that of Crz, despite stronger inhibition of AKT phosphorylation by Gef than by Crz in PC9GR cells (**Figure 3C**), suggesting the presence of an alternative mechanism underlying Gef resistance. To further investigate this, the AKT activator SC79 was added to the medium to activate the AKT signaling pathway in PC9GR cells. AO staining demonstrated that SC79 did not reverse the enhanced apoptosis or inhibition of proliferation induced by Gef + Crz treatment (**Figure 3D**). These results indicate that Gef + Crz not only suppresses AKT signaling but also engages additional pathways that promote apoptosis and inhibit proliferation, including Crz-mediated suppression of ERK activation.

We next examined p-ERK and ERK levels in PC9GR cells. Gef monotherapy increased p-ERK levels by approximately 29% compared with the control, indicating feedback activation of the ERK pathway—a key mechanism underlying Gef resistance. In contrast, Crz monotherapy reduced p-ERK levels by approximately 41%, whereas the Gef + Crz combination suppressed p-ERK by approximately 29% and effectively abrogated Gef-induced ERK activation (**Figure 3C**). For p-AKT, Gef and Crz monotherapy reduced levels by approximately 44% and 16%, respectively, compared with the control, while the combination achieved a more potent reduction of approximately 55%. These results confirm that the Gef + Crz combination synergistically inhibits resistance-related PI3K/AKT and ERK signaling pathways.

3.4. Gef + Crz synergistically inhibits the growth and metastasis of PC9GR cells in zebrafish tumor xenograft model

Encouraged by the *in vitro* antitumor efficacy, the zebrafish tumor xenograph model was employed to evaluate the therapeutic efficacy of the Gef + Crz combination *in vivo*. The construction of the xenograft model and the experimental therapeutic process are shown in **Figure 4A**. After 3 days of treatment, PC9GR cells were observed scattered within the perivitelline space (PVS) of the zebrafish. The number of tumor cells in the PVS indicated that the Gef + Crz combination significantly inhibited tumor growth (**Figure 4B** and **D**).

We also evaluated PC9GR cell metastasis by counting the number of tumor cells that metastasized to the tail using fluorescence imaging. The results showed that combination therapy significantly reduced the number of metastasized cells in the zebrafish tail compared with single-drug and control groups (**Figure 4C** and **E**).

3.5. Gef + Crz inhibits PI3K/AKT-mediated distal metastasis of PC9GR cells in zebrafish tumor xenograft model

The findings revealed that the PI3K/AKT pathway is significantly upregulated in PC9GR cells. Evidence from multiple malignancies—including lung adenocarcinoma[22-24] and melanoma[31]—supports a critical role for PI3K/AKT signaling in systemic metastasis. Bioinformatics analysis of metastatic patterns across cancers revealed a predominant association between PI3K/AKT activation and distal dissemination in lung adenocarcinoma (Figure S4).[32]

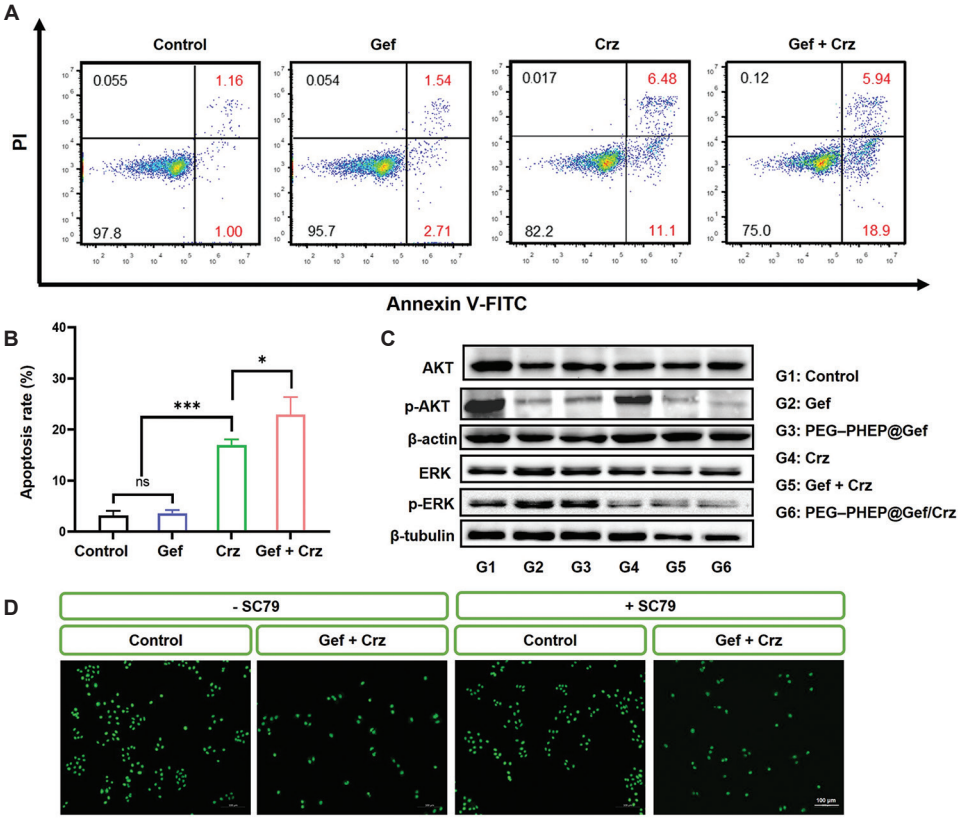

Figure 3. Gef combined with Crz synergistically inhibits PI3K–AKT signaling and suppresses ERK signaling feedback activation, inducing apoptosis in PC9GR cells. (A) Fluorescence-activated cell sorting analysis and (B) quantification of apoptosis following treatment with different formulations. (C) Immunoblot analysis of AKT, p-AKT, ERK, and p-ERK levels in PC9GR cells after treatment with different formulations. (D) Acridine orange staining of PC9GR cells with or without SC79 (scale bar = 100 μm; magnification = 10×). Data are presented as mean ± standard deviation. Statistical significance was assessed using an unpaired *t*-test. **p*<0.05 and ****p*<0.001 indicate statistical significance; "ns" indicates no significant difference.

Abbreviations: AKT: Protein kinase B; Crz: Crizotinib; ERK: Extracellular signal-regulated kinase; Gef: Gefitinib; p-AKT: Phosphorylated protein kinase B; p-ERK: Phosphorylated extracellular signal-regulated kinase; PC9GR: Gefitinib-resistant PC-9 cell; PEG: Poly (ethylene glycol); PHEP: Poly (hexyl ethylene phosphate); PI3K: Phosphatidylinositol 3-kinase.

Analysis of RNA-sequencing data from PC-9 brain-metastatic cells and parental PC-9 cells in the Gene Expression Omnibus database confirmed via KEGG pathway enrichment analysis that PI3K/AKT signaling is a central regulator of metastatic progression (**Figure 5A** and **B**). Notably, focal adhesion and extracellular matrix–receptor interaction pathways were concurrently enriched in both Gef-resistant and Gef-metastatic phenotypes (**Figures 1E** and **5B**), suggesting that these processes may functionally link therapeutic resistance and distal spread.

To quantitatively assess metastatic potential, we established a zebrafish circulating tumor cell model. Fluorescence tracking demonstrated significantly increased distal metastatic capacity in PC9GR and A549GR cells compared with their parental counterparts (**Figure 5C** and **D**). Furthermore, compared with parental A549 and PC-9 cell lines, p-AKT levels were significantly increased by 67% and 40% in A549GR and PC9GR cells, respectively (Figure S5). Building on the observed suppression of AKT phosphorylation by combination therapy, its anti-metastatic efficacy was evaluated using this model. Following the experimental scheme shown in **Figure 4A**, co-treatment with Gef and Crz reduced metastatic foci by 68.4%, outperforming Gef monotherapy (**Figure 5C** and **E**).

3.6. Nanoparticle preparation and characterization

To develop a nanocarrier for co-delivering TKIs, Gef and Crz were encapsulated in a 1:1 ratio using a PEG–PHEP amphiphilic block copolymer via nanoprecipitation and self-assembly, and the resulting nanoparticles were denoted as PEG–PHEP@Gef/Crz (**Figure 6A**). The hydrophobic PHEP inner core provides a stable environment for drug loading, while the outer hydrophilic PEG shell reduces protein adsorption and prevents rapid elimination.[33,34]

Dynamic light scattering analysis revealed that the particle size of PEG–PHEP@Gef/Crz was 40.1 ± 1.1 nm (**Figure 6B**), whereas PEG–PHEP@Gef and PEG–PHEP@Crz exhibited particle sizes of 37.5 ± 2.8 nm and 40.6 ± 2.7 nm, respectively (Figure S6). Ultraviolet-visible spectroscopy showed that PEG–PHEP@Gef and PEG–PHEP@Crz displayed the characteristic absorption peaks of Gef (332 nm) and Crz (275 nm), respectively, and that PEG–PHEP@Gef/Crz exhibited peaks corresponding to both drugs (Figure S7), indicating successful co-encapsulation. Importantly, PEG–PHEP@Gef/Crz demonstrated excellent colloidal stability in PBS, 10% FBS, and complete RPMI 1640 medium, with no significant changes in particle size (**Figure 6C**).

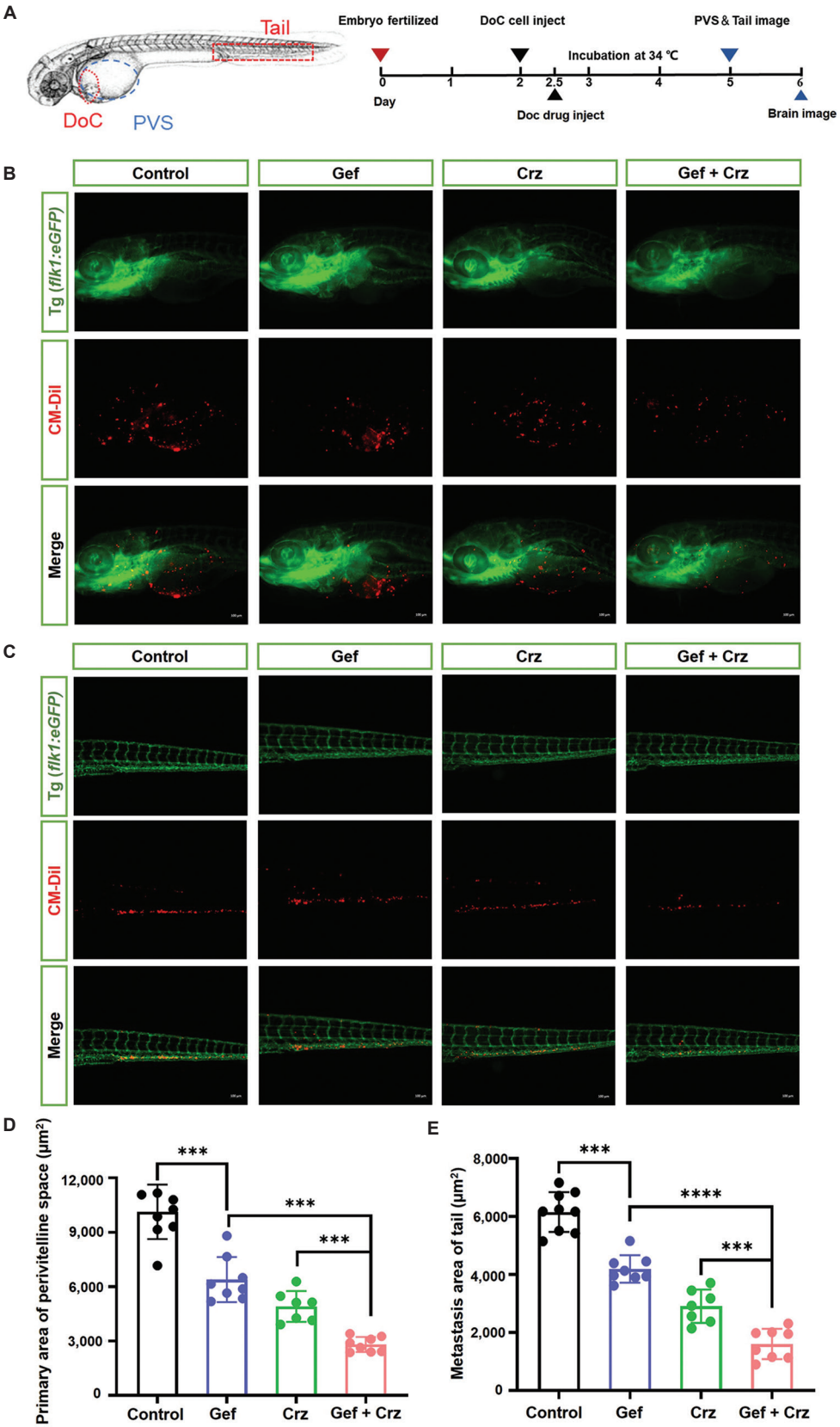

Figure 4. Gef combined with Crz synergistically inhibits the growth and metastasis of PC9GR cells in a zebrafish xenograft model. (A) Image of a 2 dpf zebrafish embryo and schematic of the experimental procedure. The DoC indicates the injection site, the PVS indicates the location of the primary tumor, and the tail indicates metastatic tumor sites. Representative images of zebrafish PC9GR tumor xenografts treated with different formulations at 5 dpf: (B) PVS images and (C) tail images (scale bar = 100 μM; magnification = 10×). Quantification of (D) primary tumor area in the PVS and (E) metastatic tumor area in the tail. Data are presented as mean ± standard deviation. Statistical significance was assessed using an unpaired Student's *t*-test. ***$p<0.001$ and ****$p<0.0001$ indicate statistical significance.

Abbreviations: Crz: Crizotinib; DoC: Duct of Cuvier; Gef: Gefitinib; PC9GR: Gefitinib-resistant PC-9 cell; PVS: Perivitelline space.

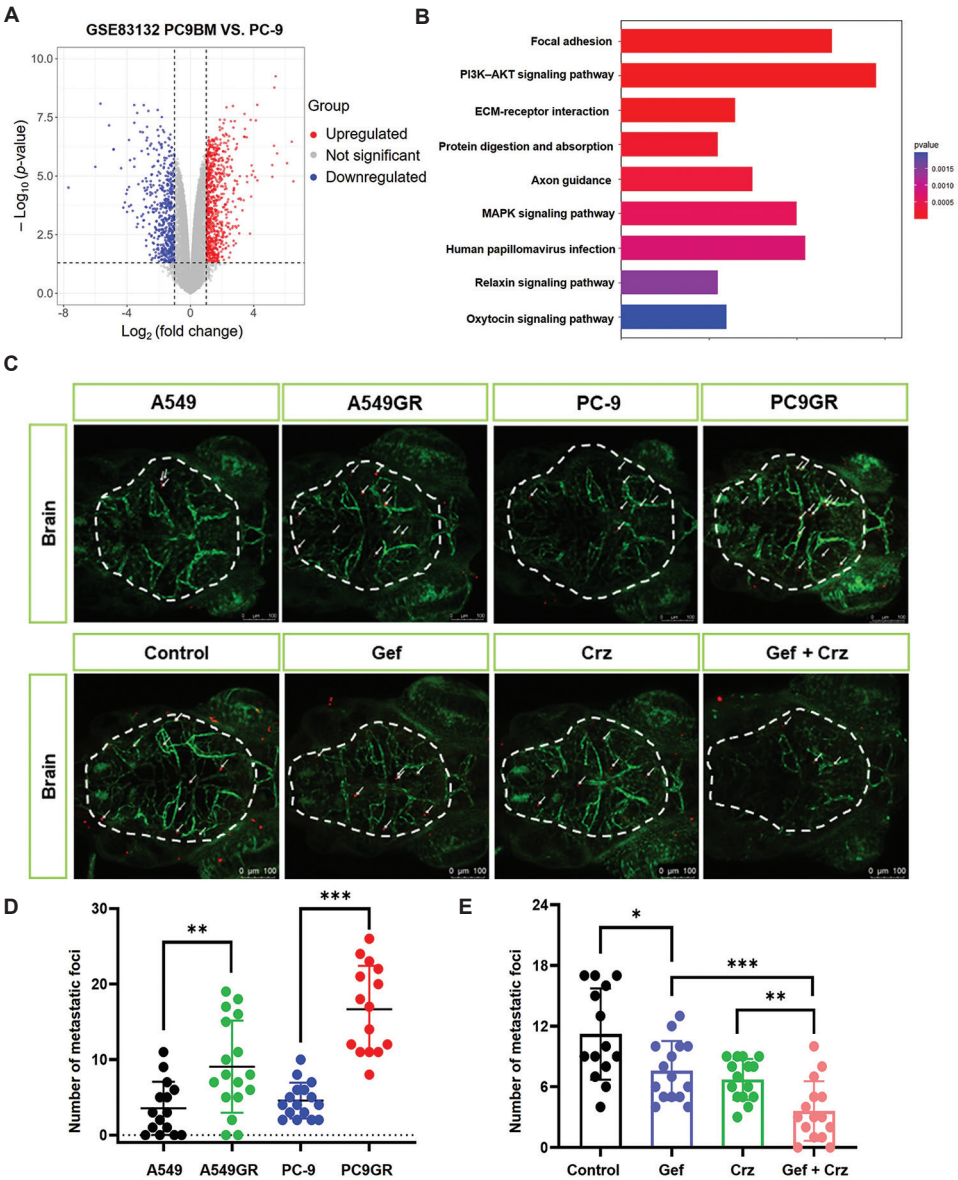

Figure 5. Gef combined with Crz inhibits PI3K–AKT-mediated distal metastasis of PC9GR cells in a zebrafish xenograft model. (A) Volcano plots showing differential gene expression between PC9GR and parental PC-9 cells in the GSE83132 dataset. (B) KEGG enrichment analysis of upregulated genes. (C) Representative brain images of zebrafish tumor xenograft models at 6 dpf derived from different cell lines (top) and treated with different formulations (bottom) (scale bar = 100 μM; magnification = 40×). (D) Quantification of the number of metastatic foci derived from different cell lines, and (E) quantification of the number of metastatic foci after treatment with different formulations. Data are presented as mean ± standard deviation. Statistical significance was assessed using an unpaired Student's *t*-test. **p*<0.05, ***p*<0.01, and ****p*<0.001 indicate statistical significance.
Abbreviations: A549GR: Gefitinib-resistant A549 cell; Crz: Crizotinib; Gef: Gefitinib; PC9GR: Gefitinib-resistant PC-9 cell.

To evaluate drug encapsulation efficiency, nanoparticles were freeze-dried, dissolved in dimethyl sulfoxide, and the drug content was quantified using high-performance liquid chromatography. The encapsulation efficiency of PEG–PHEP@Gef/Crz was 73.52% ± 5.06% and 75.17% ± 6.31% for Gef and Crz, respectively (Figure S8). These findings indicate that Gef and Crz can be effectively co-encapsulated within PEG–PHEP nanoparticles at an approximate 1:1 ratio with high encapsulation efficiency.

3.7. Cellular uptake of PEG–PHEP@Gef/Crz

Coumarin 6, a fluorescent probe commonly used in drug delivery studies,[35] was loaded into PEG–PHEP@Gef/Crz as a fluorescence indicator. To evaluate uptake efficiency, PC9GR cells were co-incubated with C6-loaded PEG–PHEP@Gef/Crz for various durations, and intracellular fluorescence was analyzed by FACS. FACS analysis of mean fluorescence intensity indicated that PC9GR cells effectively internalized PEG–PHEP@Gef/Crz within 2 h (**Figure 6D**).

Following 2 h of coincubation, CLSM analysis demonstrated that C6 fluorescence was localized at the cell membrane (**Figure 6E**), indicating effective nanoparticle uptake by PC9GR cells. Moreover, the membrane localization of C6 is consistent with the mechanism of action of Gef, which targets the cell membrane.

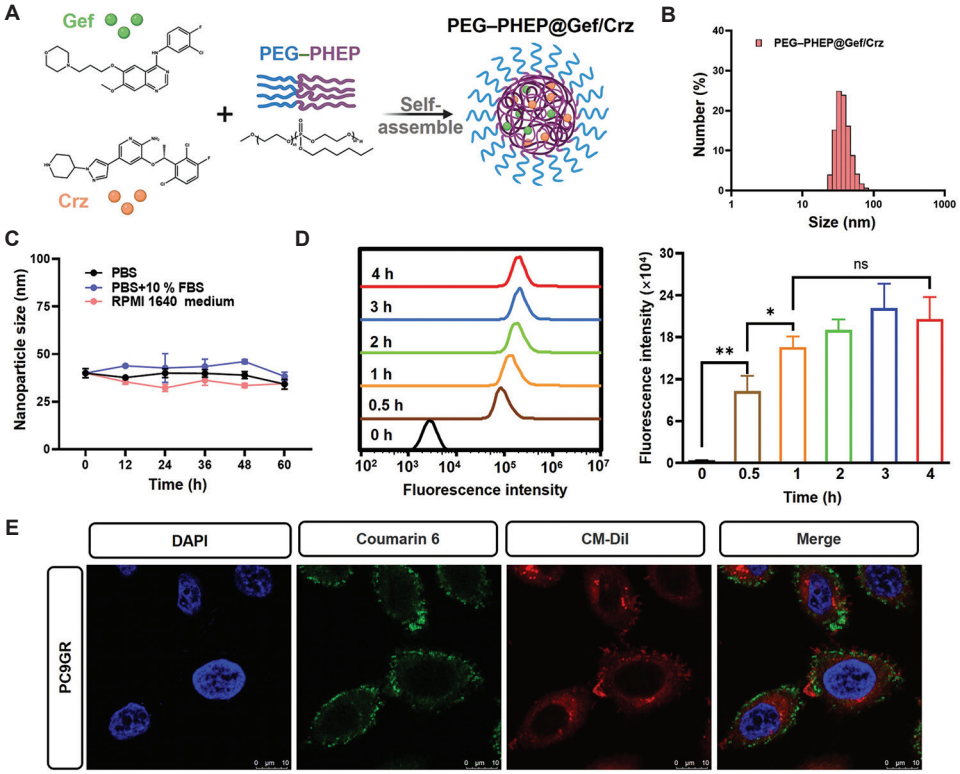

Figure 6. Characterization and cellular uptake of PEG–PHEP@Gef/Crz. (A) Schematic representation of the synthesis of PEG–PHEP@Gef/Crz. (B) Size distribution of PEG–PHEP@Gef/Crz. (C) Time-dependent stability of PEG–PHEP@Gef/Crz in PBS, PBS supplemented with 10% FBS, and complete RPMI 1640 medium. (D) Fluorescence-activated cell sorting analysis quantifying the intracellular fluorescence intensity of PC9GR cells incubated with PEG–PHEP@Gef/Crz at different time points. (E) Representative CLSM images of PC9GR cells incubated with PEG–PHEP@Gef/Crz. Cell nuclei were stained with Hoechst (blue), cell membranes were stained with DiI (red), and PEG–PHEP@Gef/Crz was labeled with Coumarin 6 (green) (scale bar =10 μm; magnification: 63×). Data are presented as mean ± standard deviation. Statistical significance was assessed using an unpaired Student's *t*-test. **p*<0.05 and ***p*<0.01 indicate statistical significance; "ns" indicates no statistical significance. Abbreviations: Crz: Crizotinib; DAPI: 4',6-diamidino-2-phenylindole; FBS: Fetal bovine serum; Gef: Gefitinib; PBS: Phosphate-buffered saline; PC9GR: Gefitinib-resistant PC-9 cell; PEG: Poly (ethylene glycol); PHEP: Poly (hexyl ethylene phosphate). **Figure 6A** was created in BioRender. Xu, B. (2025), https://BioRender.com/wt8xc37.

3.8. PEG–PHEP@Gef/Crz effectively inhibits PC9GR tumor growth and distal organ metastasis

Based on the promising *in vitro* uptake efficiency and antitumor effects of PEG–PHEP@Gef/Crz *in vitro*, we investigated its therapeutic efficacy in tumor-bearing mice. Mice harboring PC9GR tumors were intravenously administered with various formulations every 3 days at a dose of 2 mg/kg for both Gef and Crz, and tumor size and body weight were monitored post-treatment (**Figure 7A**).

Analysis of tumor size and weight revealed that PC9GR tumors were significantly resistant to PEG–PHEP@Gef, whereas PEG–PHEP@Gef/Crz demonstrated the most pronounced reduction in tumor weight and volume compared with free Gef + Crz (**Figure 7B-D**). Moreover, PEG–PHEP@Gef/Crz exhibited superior therapeutic efficacy, as evidenced by individual tumor growth curves (Figure S9). We hypothesize that the inferior efficacy of the free Gef + Crz combination treatment is due to differences in the pharmacokinetics of Gef and Crz and rapid clearance from circulation, leading to reduced drug accumulation in Gef-resistant tumors.

Further immunofluorescence analysis revealed that tumors in the PEG–PHEP@Gef/Crz treatment group exhibited enhanced apoptosis and suppressed proliferation (**Figure 7E**). H&E staining of liver and lung tissues demonstrated that PEG–PHEP@Gef/Crz almost completely inhibited PC9GR metastasis to distant organs. In contrast, metastatic foci persisted in the groups treated with nanoparticles alone or free drug combination, highlighting the improved circulation time and consistent pharmacokinetics of PEG–PHEP@Gef/Crz (**Figure 7F**).

Additionally, no significant changes in body weight were observed across treatment groups (Figure S10), and hematological and biochemical indices of liver and kidney function (Figure S11), as well as H&E-stained organs (Figure S12), showed no abnormalities, indicating that PEG–PHEP@Gef/Crz possesses good biocompatibility.

3.9. Bioinformatics analysis of the antitumor effects of PEG–PHEP@Gef/Crz

To elucidate the mechanisms underlying the antitumor effects, tumor tissues from both the PEG–PHEP@Gef/Crz and PBS groups were collected for RNA-sequencing analysis. In total, 16,319 genes were analyzed, of which 230 were upregulated, and 501 were downregulated (**Figure 8A** and **B**). GO functional annotation analysis revealed that the DEGs were significantly

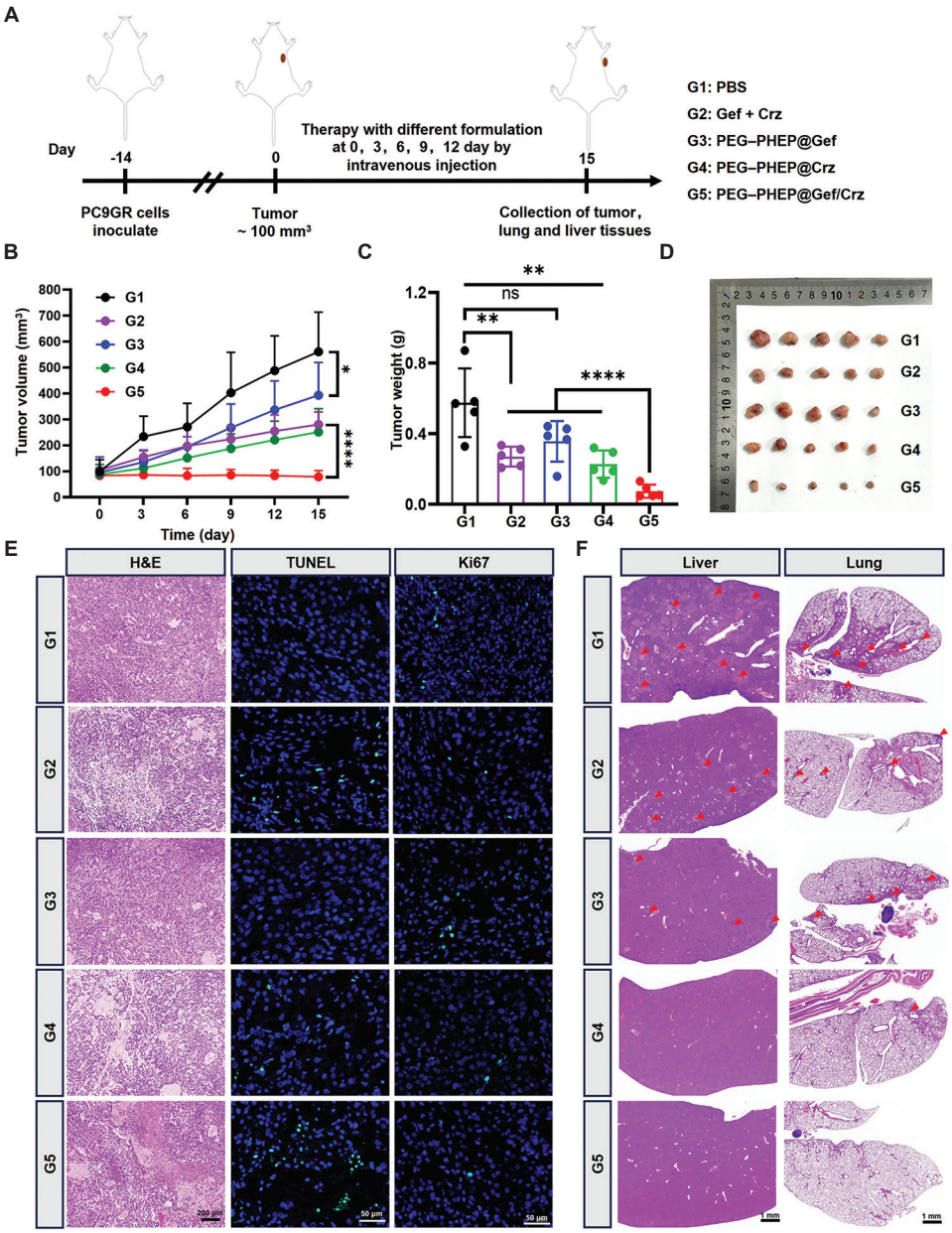

Figure 7. PEG–PHEP@Gef/Crz effectively inhibits PC9GR tumor growth and distal organ metastasis. (A) Schematic illustration of the *in vivo* antitumor experiment in nude mice. Mice were intravenously administered Gef (2 mg/kg) and Crz (2 mg/kg). Growth curves of PC9GRxenograft (B) tumor volume and (C) tumor weight measured over a 15-day treatment period. (D) Representative images of excised tumor tissues following treatment. (E) Representative images of H&E staining, TUNEL assay, and Ki67 immunofluorescence staining of tumor tissues following treatment (scale bar = 50 μm; magnification = 20×). (F) Representative images of H&E-stained liver and lung tissues following treatment (scale bar = 1 mm; magnification = 3×). Data are presented as mean ± standard deviation. Statistical significance was assessed using an unpaired Student's *t*-test. *$p<0.05$, **$p<0.01$, and ****$p<0.0001$ indicate statistical significance; "ns" indicates no statistical significance.
Abbreviations: Crz: Crizotinib; H&E: Hematoxylin and eosin; PC9GR: Gefitinib-resistant PC-9 cell; PEG: Poly (ethylene glycol); PHEP: Poly (hexyl ethylene phosphate); TUNEL: Terminal deoxynucleotidyl transferase-mediated dUTP nick-end labeling.

associated with biological processes such as negative regulation of cell migration, negative regulation of cell motility, integrin-mediated cell adhesion, wound healing, and the ERK signaling cascade (**Figure 8C**). These DEGs were also involved in molecular functions such as cytokine activity, growth factor activity, and cytokine receptor binding (**Figure 8C**). These processes are predominantly implicated in the regulation of tumor growth and metastasis, providing a molecular basis for the observed inhibition of growth and distal metastasis in PC9GR tumors following treatment with PEG–PHEP@Gef/Crz. KEGG pathway analysis further revealed that DEGs were enriched in pathways related to cytokine–cytokine receptor interaction, nuclear factor κ-light-chain-enhancer of activated B cells signaling, cell adhesion molecules, apoptosis, PI3K/AKT signaling, and mitogen-activated protein kinase signaling (**Figure 8D**).

Furthermore, we conducted an additional analysis of the expression changes of key tumor drug resistance-related genes following treatment. The results demonstrated that the

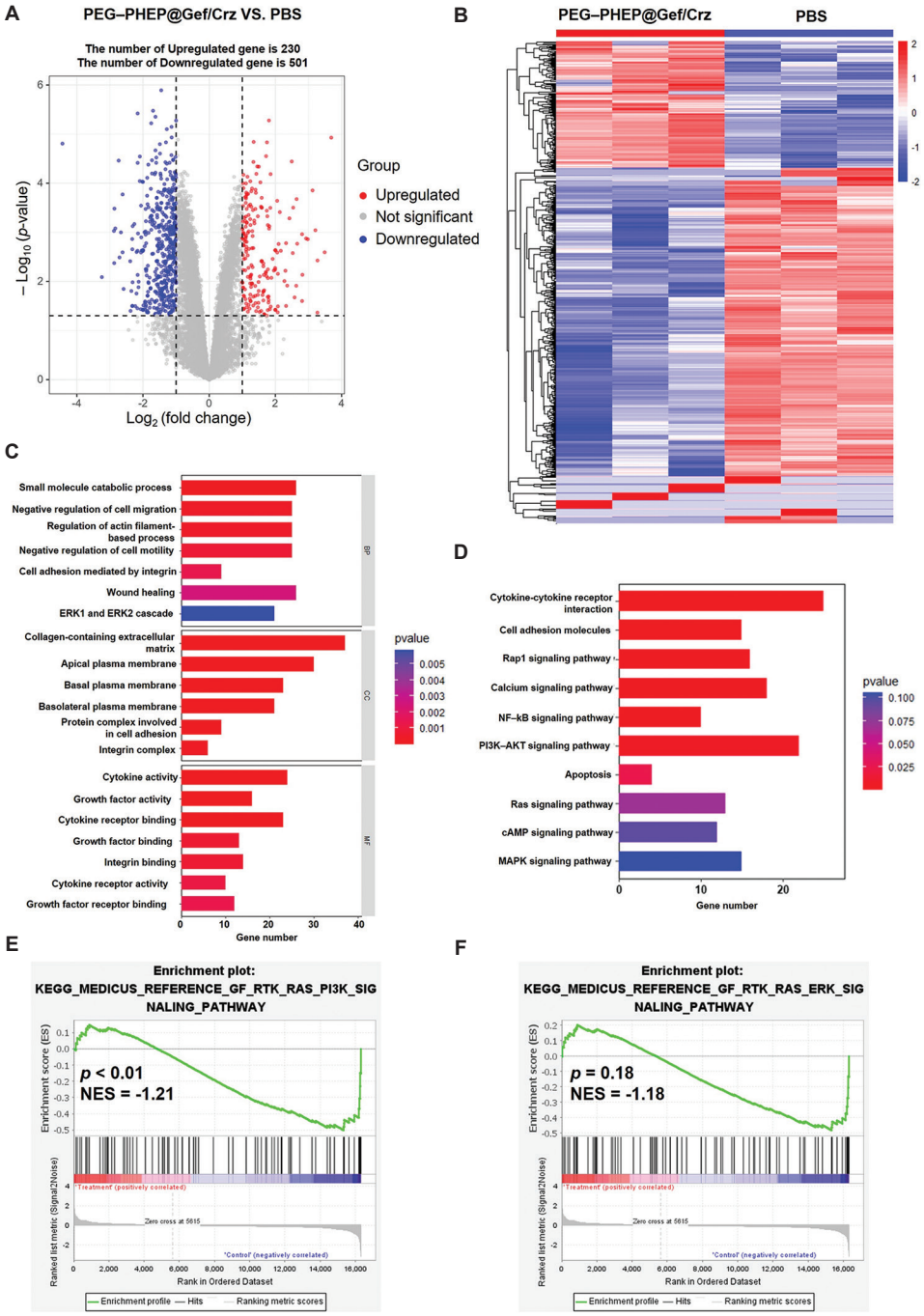

Figure 8. mRNA sequence analysis of PEG–PHEP@Gef/Crz-treated tumors. (A) Volcano plot showing differentially expressed genes, including 230 upregulated genes and 501 downregulated genes, following PEG–PHEP@Gef/Crz treatment. (B) Heatmap of 731 differential expressed genes. (C) Gene Oncology annotation and (D) Kyoto Encyclopedia of Genes and Genomes enrichment analysis of the differentially expressed genes. Gene set enrichment analysis of (E) RTK/RAS/PI3K and (F) RTK/RAS/ERK signaling pathways following PEG–PHEP@Gef/Crz treatment.

Abbreviations: Crz: Crizotinib; ERK: Extracellular signal-regulated tyrosine kinase; PBS: Phosphate-buffered saline; PC9GR: Gefitinib-resistance PC-9 cell; PEG: Poly (ethylene glycol); PHEP: Poly (hexyl ethylene phosphate); PI3K: Phosphatidylinositol 3-kinase; RAS: Rat sarcoma virus oncogene family; RTK: Receptor tyrosine kinase.

expression levels of EGFR, Kirsten rat sarcoma viral oncogene homolog, EMT factors, and B-Raf proto-oncogene, serine/threonine kinase did not exhibit significant upregulation (Figure S13), indicating that the mechanism underlying drug resistance reversal primarily involves direct inhibition of downstream signaling activation.

To substantiate the proposed mechanism of synergistic Gef and Crz treatment, we performed GSEA analysis. The findings revealed a significant reduction in PI3K/AKT and RAS/ERK signaling pathways following treatment (**Figure 8E** and **F**), indicating that PEG–PHEP@Gef/Crz synergistically suppresses overactivation of PI3K/AKT signaling in drug-resistant lung

adenocarcinoma. Additionally, it effectively mitigates feedback activation of the ERK signaling pathway. Collectively, these effects potently induce apoptosis and reverse drug resistance, underscoring the therapeutic potential of PEG–PHEP@Gef/Crz for overcoming treatment resistance in lung cancer.

4. Discussion

Numerous EGFR-TKI drugs have been developed for the clinical management of EGFR-driven lung cancer, demonstrating considerable efficacy.[11] However, the emergence of acquired tumor resistance remains a major limitation to the therapeutic application of these molecularly targeted agents.[36] Combination therapy has been shown to reverse tumor resistance to monotherapy by targeting multiple pivotal signaling pathways critical for tumor survival.[37] However, the antitumor efficacy of free drugs remains suboptimal due to poor *in vivo* circulation, limited tumor targeting, minimal tumor accumulation, and variable pharmacokinetics.[38] Consequently, enhancing the efficiency of molecularly targeted drug delivery and overcoming tumor drug resistance are pivotal for improving antitumor outcomes.

In this study, we first analyzed publicly available RNA sequencing datasets, followed by protein-level experiments to confirm overactivation of the PI3K/AKT signaling cascade in PC9GR cells. Overactivation of PI3K/AKT signaling has been reported as a key factor in the development of EGFR-TKI resistance.[39,40]

Numerous studies have proposed diverse combination strategies to combat EGFR-TKI resistance, aiming to identify Food and Drug Administration-approved first-line therapies for NSCLC. Crz serves as a frontline therapy for patients with anaplastic lymphoma kinase-mutated NSCLC. Notably, suppression of the PI3K/AKT signaling pathway has been documented in both neuroblastoma and pancreatic cancer.[41,42] Therefore, we proposed a therapeutic strategy combining Gef with Crz.

Furthermore, we discovered a strong synergistic effect when Grf and Crz were used at a 1:1 ratio, and this combination therapy significantly inhibited the proliferation and migration of PC9GR cells. Mechanistically, this co-treatment induced apoptosis by synergistically reducing AKT phosphorylation and concurrently suppressing feedback activation of the ERK signaling pathway. Using a zebrafish tumor xenograft model, we further demonstrated the inhibitory effect of this combination on PC9GR tumor growth and metastasis.

Although previous studies have implicated PI3K/AKT signaling in organotrophic metastasis,[22,24] our integrated analysis of RNA sequencing data from metastatic PC-9 brain-metastatic cells and parental PC-9 revealed a central role for this pathway in enhancing metastatic competence. Quantitative assessment using whole-body fluorescence imaging revealed a significantly increased metastatic burden in resistant cells compared with parental controls. Notably, pharmacological co-targeting achieved superior metastasis control relative to single-drug treatment. These findings suggest that PI3K/AKT signaling functions as a key driver of both therapeutic resistance and metastatic progression, although the spatiotemporal regulation of this pathway during the dissemination cascade warrants further investigation.

Despite the notable efficacy demonstrated by the combination of Crz with EGFR-TKIs in our study, this approach has not shown clear advantages in clinical settings. In a real-world study involving 70 patients with *MET*-amplified, EGFR-TKI–resistant NSCLC, the objective response rates for the group treated with EGFR-TKI + Crz compared with Crz monotherapy were 48.6% and 40%, respectively. However, no significant difference in overall survival was observed between the two treatment groups.[43] The modest outcomes are largely attributed to unsynchronized pharmacokinetics, inconsistent *MET* amplification diagnostics, and increased risk of hepatic toxicity. An observational study has indicated that simultaneous inhibition of AKT signaling and the cell cycle regulator WEE1 synergistically suppressed melanoma growth, whereas sequential administration did not yield the same beneficial outcomes.[44]

To address these challenges, we employed nanocarriers for the co-delivery of Gef and Crz in a molecularly targeted combination therapy approach. Amphiphilic block copolymers were used to co-encapsulate Gef and Crz, resulting in PEG–PHEP@Gef/Crz nanoparticles. These nanoparticles, with diameters of approximately 40 nm, effectively encapsulated both Gef and Crz in their inner core, achieving high encapsulation efficiencies of approximately 74.35%. This strategy facilitates synergistic *in vivo* co-administration of the two drugs and enhances their accumulation in tumor tissues via the enhanced permeability and retention effect, while maintaining robust dual inhibition of the PI3K/AKT and ERK pathways. Overall, this nano-co-delivery approach directly mitigates the pharmacological and clinical limitations of conventional combination therapy, thereby providing a more viable pathway toward clinical translation.

Notably, the nanoparticles were rapidly and efficiently internalized by PC9GR cells and accumulated at the cell membrane, consistent with the drugs targeting intracellular structural domains. In a mouse xenograft tumor model, we observed a pronounced tumor-suppressive effect of PEG–PHEP@Gef/Crz, which exceeded that of the free drug combination group. Cytological analyses demonstrated that PEG–PHEP@Gef/Crz more potently inhibited cell proliferation and induced apoptosis. In addition, PEG–PHEP@Gef/Crz significantly suppressed metastasis of PC9GR tumors to the liver and lungs, likely partly due to its long-circulation properties.

In summary, these findings suggest that simultaneously targeting multiple key survival signals in tumors represents an optimal strategy for overcoming small-molecule drug resistance. We also propose drug delivery strategies that extend beyond EGFR-TKIs to include other small-molecule therapeutics. Future research should focus on optimizing drug formulations and delivery strategies. Seamless integration of nanomedicine with basic oncology research is crucial to maximize the effectiveness of combination therapies and develop strategies to combat drug resistance in clinical settings.

5. Conclusions

In summary, the *in vivo* findings of this study are consistent with the *in vitro* findings, confirming that the combination of Gef and Crz enables a potent dual-pathway blockade of PI3K/AKT and ERK signaling, overcomes Gef resistance, and significantly inhibits tumor metastasis. From a translational perspective, this co-delivery strategy optimizes drug pharmacokinetics, enhances tumor accumulation via the enhanced permeability and retention effect, and maximizes synergistic efficacy, thereby effectively addressing the limitations of free-drug combinations. These findings establish nano co-delivery as a promising strategy for overcoming drug resistance and metastatic progression in EGFR-mutant lung adenocarcinoma.

Acknowledgement

We sincerely thank Professor Yiyue Zhang for kindly providing the zebrafish strains, which were instrumental in the successful completion of this study.

Financial support

This work was supported by the National Natural Science Foundation of China (82472064), the International Science and Technology Cooperation Program of Guangdong (2022A0505050048), the Natural Science Foundation of Guangdong (2024A1515012369), and the Beijing Xisike Clinical Oncology Research Foundation (Y-HS202102-0038).

Conflicts of interest statement

The authors declare no conflicts of interest.

Author contributions

Conceptualization: JD and BX; *Data curation:* HW, CW and YZ; *Investigation*: WL and HH; *Methodology:* SL, YH and ZL; *Supervision:* HZ, FZ and LY; *Writing–original draft:* JD and HQ; *Writing-review & editing:* BX and QL. All authors examined and consented to the final edition of the manuscript.

Ethics approval and consent to participate

All animal experimental procedures were conducted in accordance with relevant ethical guidelines and were approved by the Ethics Review Committee of Guangdong Provincial People's Hospital (ethics approval number: KY2023-1003-01).

Consent for publication

Not applicable.

Availability of data

Data supporting the findings of this study are available from the corresponding author upon reasonable request.

Further disclosure

The graphical abstract was created in BioRender. Xu, B. (2025), https://BioRender.com/e74v656.

References

1. Siegel RL, Miller KD, Fuchs HE, Jemal A. Cancer statistics, 2022. *CA Cancer J Clin.* 2022;72(1):7-33. doi: 10.3322/caac.21708
2. Bender E. Epidemiology: The dominant malignancy. *Nature.* 2014;513(7517):S2-S3. doi: 10.1038/513S2a
3. Shah MP, Neal JW. Targeting acquired and intrinsic resistance mechanisms in epidermal growth factor receptor mutant non-small-cell lung cancer. *Drugs.* 2022;82(6):649-662. doi: 10.1007/s40265-022-01698-z
4. Holohan C, Van Schaeybroeck S, Longley DB, Johnston PG. Cancer drug resistance: An evolving paradigm. *Nat Rev Cancer.* 2013;13(10):714-726. doi: 10.1038/nrc3599
5. Yu W, Ye F, Yuan X, *et al.* A phase I/II clinical trial on the efficacy and safety of NKT cells combined with gefitinib for advanced EGFR-mutated non-small-cell lung cancer. *BMC Cancer.* 2021;21(1):877. doi: 10.1186/s12885-021-08590-1
6. Han W, Shi L, Ren L, *et al.* A nanomedicine approach enables co-delivery of cyclosporin A and gefitinib to potentiate the therapeutic efficacy in drug-resistant lung cancer. *Signal Transduct Target Ther.* 2018;3:16. doi: 10.1038/s41392-018-0019-4
7. Zhao L, Yang G, Shi YJ, Su C, Chang J. Co-delivery of Gefitinib and chloroquine by chitosan nanoparticles for overcoming the drug acquired resistance. *J Nanobiotechnology.* 2015;13:57. doi: 10.1186/s12951-015-0121-5
8. Liu Y, Dai X, Jiang S, *et al.* Targeted co-delivery of gefitinib and rapamycin by aptamer-modified nanoparticles overcomes EGFR-TKI resistance in NSCLC via promoting autophagy. *Int J Mol Sci.* 2022;23(14):8025. doi: 10.3390/ijms23148025
9. Wu Y, Cheng Y, Zhou J, *et al.* Tepotinib plus gefitinib in patients with EGFR-mutant non-small-cell lung cancer with MET overexpression or MET amplification and acquired resistance to previous EGFR inhibitor (INSIGHT study): An open-label, phase 1b/2, multicentre, randomised trial. *Lancet Respir Med.* 2020;8(11):1132-1143. doi: 10.1016/S2213-2600(20)30154-5
10. Li S, Zeng F, Zhou Q, *et al.* NIR-II photoacoustic imaging-guided chemo-photothermal therapy using PA1094T combined with anti-CD47 antibody: Activating pyroptosis against orthotopic glioblastoma. *Adv Healthc Mater.* 2025;14(3):e2403108. doi: 10.1002/adhm.202403108
11. Xu B, Zeng F, Deng J, *et al.* A homologous and molecular dual-targeted biomimetic nanocarrier for EGFR-related non-small cell lung cancer therapy. *Bioact Mater.* 2023;27:337-347. doi: 10.1016/j.bioactmat.2023.04.005
12. Qu J, Li J, Zhang Y, *et al.* AKR1B10 promotes breast cancer cell proliferation and migration via the PI3K/AKT/NF-κB signaling pathway. *Cell Biosci.* 2021;11(1):163. doi: 10.1186/s13578-021-00677-3
13. Si X, Xu F, Xu F, Wei M, Ge Y, Chenge S. CADM1 inhibits ovarian cancer cell proliferation and migration by potentially regulating the PI3K/Akt/mTOR pathway. *Biomed Pharmacother.* 2020;123:109717. doi: 10.1016/j.biopha.2019.109717
14. Hu C, Zha Q, Hua P, Xiao L, Pan D. NUCKS promotes the proliferation, migration and invasion of lung cancer cells through Pi3k/Akt signaling pathway. *Clin Invest Med.* 2021;44(2):E55-E61. doi: 10.25011/cim.v44i2.36246
15. Yu L, Wei J, Liu P. Attacking the PI3K/Akt/mTOR signaling pathway for targeted therapeutic treatment in human cancer. *Semin Cancer Biol.* 2022;85:69-94. doi: 10.1016/j.semcancer.2021.06.019
16. Hao J, Zhang W, Huang Z. Bupivacaine modulates the apoptosis and ferroptosis in bladder cancer via phosphatidylinositol 3-kinase (PI3K)/AKT pathway. *Bioengineered.* 2022;13(3):6794-6806. doi: 10.1080/21655979.2022.2036909
17. Gao H, Wang W, Li Q. GANT61 suppresses cell survival, invasion and epithelial-mesenchymal transition through inactivating AKT/mTOR and JAK/STAT3 pathways in anaplastic thyroid carcinoma. *Cancer Biol Ther.* 2022;23(1):369-377. doi: 10.1080/15384047.2022.2051158
18. Ding J, Ding X, Leng Z. LPCAT1 promotes gefitinib resistance via upregulation of the EGFR/PI3K/AKT signaling pathway in lung adenocarcinoma. *J Cancer.* 2022;13(6):1837-1847. doi: 10.7150/jca.66126
19. Deng Q, Fang Q, Ji X, Zhou S. Cyclooxygenase-2 mediates Gefitinib resistance in non-small cell lung cancer through the EGFR/PI3K/AKT axis. *J Cancer.* 2020;11(12):3667-3674. doi: 10.7150/jca.42850
20. Zaryouh H, De Pauw I, Baysal H, *et al.* Recent insights in the PI3K/Akt pathway as a promising therapeutic target in combination with EGFR-targeting agents to treat head and neck squamous cell carcinoma. *Med Res*

Rev. 2022;42(1):112-155.
doi: 10.1002/med.21806
21. Sato H, Yamamoto H, Sakaguchi M, *et al.* Combined inhibition of MEK and PI3K pathways overcomes acquired resistance to EGFR-TKIs in non-small cell lung cancer. *Cancer Sci.* 2018;109(10):3183-3196.
doi: 10.1111/cas.13763
22. Wei C, Dong X, Lu H, *et al.* LPCAT1 promotes brain metastasis of lung adenocarcinoma by up-regulating PI3K/AKT/MYC pathway. *J Exp Clin Cancer Res.* 2019;38(1):95.
doi: 10.1186/s13046-019-1092-4
23. Zhu L, Yang F, Wang G, Li Q. CXC motif chemokine receptor type 4 disrupts blood-brain barrier and promotes brain metastasis through activation of the PI3K/AKT pathway in lung cancer. *World Neurosurg.* 2022;166:e369-e381.
doi: 10.1016/j.wneu.2022.07.005
24. Li Q, Yang J, Yu Q, *et al.* Associations between single-nucleotide polymorphisms in the PI3K-PTEN-AKT-mTOR pathway and increased risk of brain metastasis in patients with non-small cell lung cancer. *Clin Cancer Res.* 2013;19(22):6252-6260.
doi: 10.1158/1078-0432.CCR-13-1093
25. Park S, Cho EA, Chun JN, *et al.* Crizotinib attenuates cancer metastasis by inhibiting TGFβ signaling in non-small cell lung cancer cells. *Exp Mol Med.* 2022;54(8):1225-1235.
doi: 10.1038/s12276-022-00835-8
26. Xu W, Kim JW, Jung WJ, Koh Y, Yoon SS. Crizotinib in combination with everolimus synergistically inhibits proliferation of anaplastic lymphoma kinase-positive anaplastic large cell lymphoma. *Cancer Res Treat.* 2018;50(2):599-613.
doi: 10.4143/crt.2016.357
27. Megiorni F, McDowell HP, Camero S, *et al.* Crizotinib-induced antitumour activity in human alveolar rhabdomyosarcoma cells is not solely dependent on ALK and MET inhibition. *J Exp Clin Cancer Res.* 2015;34:112.
doi: 10.1186/s13046-015-0228-4
28. Wang X, Cao J, Du W, Zhang W, Cao S. Response to gefitinib/crizotinib combination in a pulmonary sarcomatoid carcinoma patient harboring concurrent EGFR mutation and MET amplification. *Clin Case Rep.* 2021;9(7):e04487.
doi: 10.1002/ccr3.4487
29. Li D, Wang J, Ma Y, *et al.* A donor-acceptor conjugated polymer with alternating isoindigo derivative and bithiophene units for near-infrared modulated cancer thermo-chemotherapy. *ACS Appl Mater Interfaces.* 2016;8(30):19312-19320.
doi: 10.1021/acsami.6b05495
30. Shou J, You L, Yao J, *et al.* Cyclosporine A sensitizes human non-small cell lung cancer cells to gefitinib through inhibition of STAT3. *Cancer Lett.* 2016;379(1):124-133.
doi: 10.1016/j.canlet.2016.06.002
31. Tehranian C, Fankhauser L, Harter PN, *et al.* The PI3K/Akt/mTOR pathway as a preventive target in melanoma brain metastasis. *Neuro Oncol.* 2022;24(2):213-225.
doi: 10.1093/neuonc/noab159
32. Jiang B, Mu Q, Qiu F, *et al.* Machine learning of genomic features in organotropic metastases stratifies progression risk of primary tumors. *Nat Commun.* 2021;12(1):6692.
doi: 10.1038/s41467-021-27017-w
33. Hu Y, Zhao Z, Harmon T, Pentel PR, Ehrich M, Zhang C. Paradox of PEGylation in fabricating hybrid nanoparticle-based nicotine vaccines. *Biomaterials.* 2018;182:72-81.
doi: 10.1016/j.biomaterials.2018.08.015
34. Zhu Y, Chen C, Cao Z, *et al.* On-demand PEGylation and dePEGylation of PLA-based nanocarriers *via* amphiphilic mPEG-*TK*-Ce6 for nanoenabled cancer chemotherapy. *Theranostics.* 2019;9(26):8312-8320.
doi: 10.7150/thno.37128
35. Pretor S, Bartels J, Lorenz T, *et al.* Cellular uptake of coumarin-6 under microfluidic conditions into HCE-T cells from nanoscale formulations. *Mol Pharm.* 2015;12(1):34-45.
doi: 10.1021/mp500401t
36. Glaviano A, Foo ASC, Lam HY, *et al.* PI3K/AKT/mTOR signaling transduction pathway and targeted therapies in cancer. *Mol Cancer.* 2023;22(1):138.
doi: 10.1186/s12943-023-01827-6
37. Wei Q, Li P, Yang T, *et al.* The promise and challenges of combination therapies with antibody-drug conjugates in solid tumors. *J Hematol Oncol.* 2024;17(1):1.
doi: 10.1186/s13045-023-01509-2
38. Manzari MT, Shamay Y, Kiguchi H, Rosen N, Scaltriti M, Heller DA. Targeted drug delivery strategies for precision medicines. *Nat Rev Mater.* 2021;6(4):351-370.
doi: 10.1038/s41578-020-00269-6
39. Liu Q, Yu S, Zhao W, Qin S, Chu Q, Wu K. EGFR-TKIs resistance via EGFR-independent signaling pathways. *Mol Cancer.* 2018;17(1):53.
doi: 10.1186/s12943-018-0793-1
40. Fang W, Huang Y, Gu W, *et al.* PI3K-AKT-mTOR pathway alterations in advanced NSCLC patients after progression on EGFR-TKI and clinical response to EGFR-TKI plus everolimus combination therapy. *Transl Lung Cancer Res.* 2020;9(4):1258-1267.
doi: 10.21037/tlcr-20-141
41. Moore NF, Azarova AM, Bhatnagar N, *et al.* Molecular rationale for the use of PI3K/AKT/mTOR pathway inhibitors in combination with crizotinib in ALK-mutated neuroblastoma. *Oncotarget.* 2014;5(18):8737-8749.
doi: 10.18632/oncotarget.2372
42. Yan H, Jung K, Son M, *et al.* Crizotinib exhibits antitumor activity by targeting ALK signaling not c-MET in pancreatic cancer. *Oncotarget.* 2014;5(19):9150-9168.
doi: 10.18632/oncotarget.2363
43. Liu L, Qu J, Heng J, *et al.* A large real-world study on the effectiveness of the combined inhibition of EGFR and MET in EGFR-mutant non-small-cell lung cancer after development of EGFR-TKI resistance. *Front Oncol.* 2021;11:722039.
doi: 10.3389/fonc.2021.722039
44. Dinavahi SS, Noory MA, Gowda R, *et al.* Moving synergistically acting drug combinations to the clinic by comparing sequential versus simultaneous drug administrations. *Mol Pharmacol.* 2018;93(3):190-196.
doi: 10.1124/mol.117.110759

Received: September 6, 2025
Revised: November 9, 2025
Accepted: November 18, 2025
Available online: February 23, 2026